Biophysical mechanisms underlying olfactory receptor neuron dynamics
Katherine I. Nagel and Rachel I. Wilson

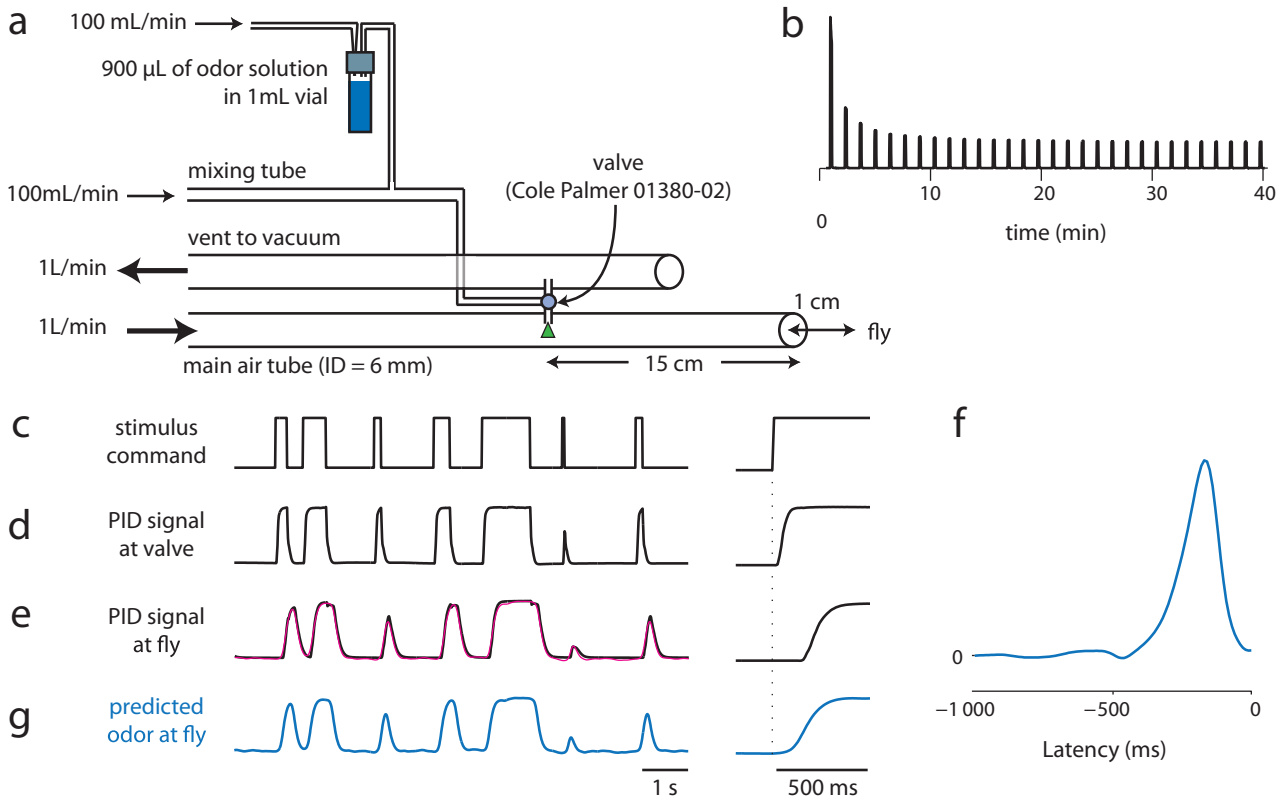

Supplementary Figure 1: Design, performance, and modeling of the odor delivery device.

(a) Design of the olfactometer. Important features are (1) continuous airflow over odor vial maintains a constant odor concentration for repeated stimulus presentations, (2) small headspace in odor vial decreases time to reach steady state concentration, and (3) balanced airflow in delivery and vacuum tubes minimizes pressure transients when the valve switches from one tube to the other.

(b) Odor device output as a function of time, measured with a photo-ionization detector (miniPID, Aurora Scientific). The odor vial (containing 2-butanone 0.1×) was placed into the device at time zero. Odor pulses (10 s duration) were delivered every 80 s. The odor concentration drops rapidly, then reaches a steady state within minutes. Based on this data, we waited 20 min after placing an odor into the device before delivering odor to the fly and beginning data collection for filter experiments. For experiments with shorter odor presentation times, we waited a fixed amount of time (3-5 min) before odor presentation. During this time air flows continuously through the odor vial and is vented through the valve to the vacuum line.

(c) Command to the valve, created from binary random values sampled at 20 Hz, passed through an exponential low-pass filter with a time constant of 3 s, then rounded to obtain a binary signal.

(d-g) To estimate the time course of odor delivered to fly, we compared the PID signal (d) recorded inside the barrel of the valve (see green arrowhead in a) to the PID signal at the fly (e, black) and computed the linear filter that best relates the signal at the valve to the signal at the fly (f). We tested this model by using it to predict the signal at the fly from the signal at the valve (magenta trace in e). This was a conservative estimate of how much the delivery device smoothed the signal because we assumed that the small difference between the command signal (c) and the signal at the valve (d) was due to the dynamics of the PID itself, while the larger difference between the signals at the valve (d) and at the fly (e) represented the time course of odor propagation from the valve to the fly. To estimate the odor delivered to the fly independent of PID dynamics, we convolved the filter model with the original command signal (c). This produced the signal shown in (g), and this was taken to be the stimulus in all experiments. The assumption of linearity in the odor delivery device is valid because the correlation between the recorded signal and predicted signal (black and magenta in e) is very high (0.995).

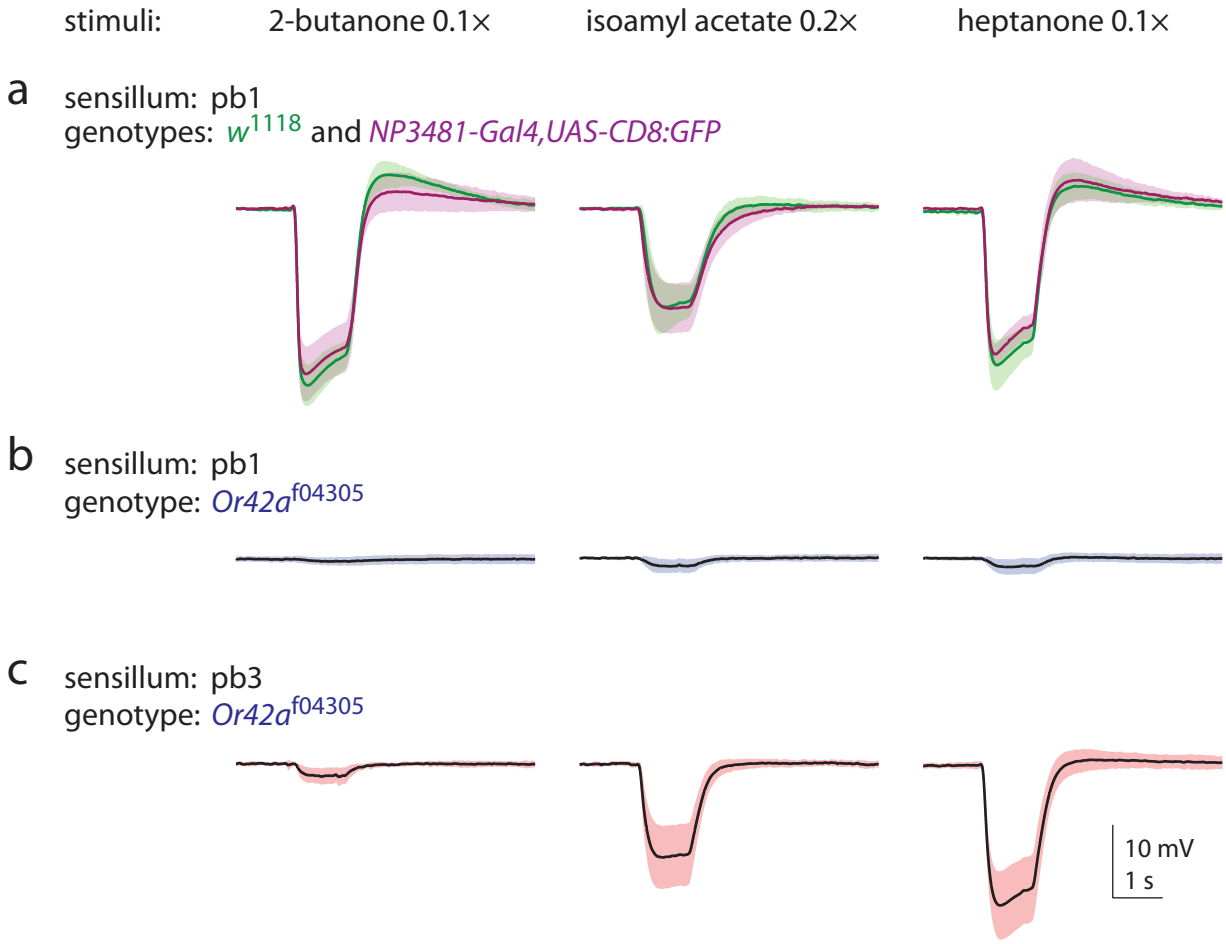

Supplementary Figure 2: Palp sensilla are relatively electrically isolated from one another.

(a) Average LFP responses of pb1 sensilla to three stimuli in two control genotypes. Each trace represents the mean of 5-15 recordings, ± s.d. across recordings.
(b) When *Or42a* is mutated, LFP responses to these stimuli in this sensillum are largely abolished. This indicates that these responses arise from the pb1A neuron.
(c) In the same genotype, responses to some of these stimuli persist in a different sensillum type (pb3). This indicates that signals arising from other palp sensilla have little or no impact on the LFP signal recorded within a single palp sensillum, at least within this range of signal amplitudes. We found that antennal sensilla are not as well-isolated as palp sensilla.

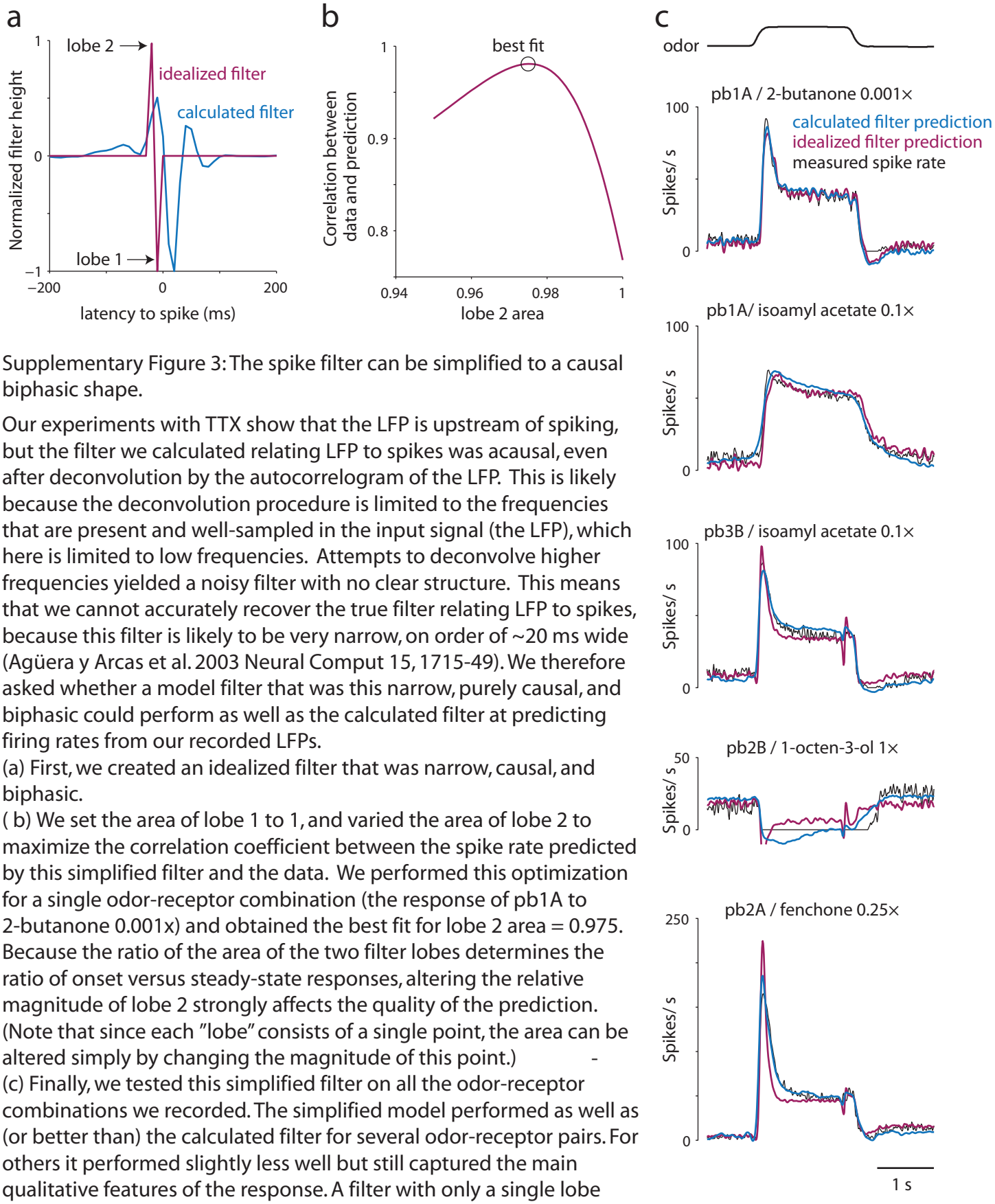

Supplementary Figure 3: The spike filter can be simplified to a causal biphasic shape.

Our experiments with TTX show that the LFP is upstream of spiking, but the filter we calculated relating LFP to spikes was acausal, even after deconvolution by the autocorrelogram of the LFP. This is likely because the deconvolution procedure is limited to the frequencies that are present and well-sampled in the input signal (the LFP), which here is limited to low frequencies. Attempts to deconvolve higher frequencies yielded a noisy filter with no clear structure. This means that we cannot accurately recover the true filter relating LFP to spikes, because this filter is likely to be very narrow, on order of ~20 ms wide (Agüera y Arcas et al. 2003 Neural Comput 15, 1715-49). We therefore asked whether a model filter that was this narrow, purely causal, and biphasic could perform as well as the calculated filter at predicting firing rates from our recorded LFPs.

(a) First, we created an idealized filter that was narrow, causal, and biphasic.

(b) We set the area of lobe 1 to 1, and varied the area of lobe 2 to maximize the correlation coefficient between the spike rate predicted by this simplified filter and the data. We performed this optimization for a single odor-receptor combination (the response of pb1A to 2-butanone 0.001x) and obtained the best fit for lobe 2 area = 0.975. Because the ratio of the area of the two filter lobes determines the ratio of onset versus steady-state responses, altering the relative magnitude of lobe 2 strongly affects the quality of the prediction. (Note that since each "lobe" consists of a single point, the area can be altered simply by changing the magnitude of this point.)

(c) Finally, we tested this simplified filter on all the odor-receptor combinations we recorded. The simplified model performed as well as (or better than) the calculated filter for several odor-receptor pairs. For others it performed slightly less well but still captured the main qualitative features of the response. A filter with only a single lobe performed poorly (not shown). Based on this analysis, we conclude that the transformation from LFP to spikes is well-described by a narrow causal biphasic filter.

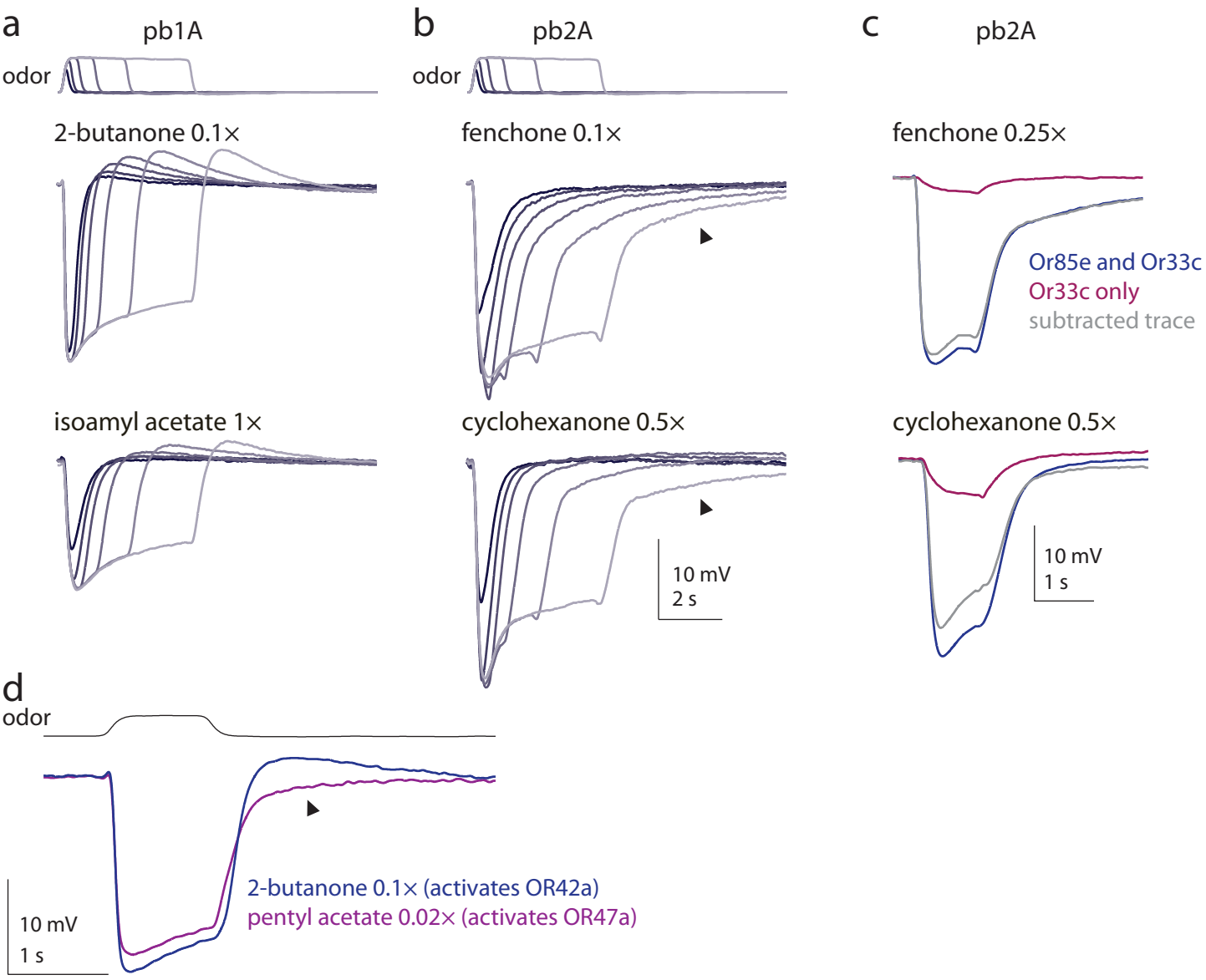

Supplementary Figure 4: A second, slow LFP decay phase is characteristic of some odorant receptors.

(a) pb1A (which expresses OR42A) shows LFP overshoot after odor offset in response to two representative stimuli. Overshoot grows with pulse duration (family of pulse durations at top).
(b) pb2A (which expresses Or85e and Or33c) does not show overshoot, and instead shows a second, slower decay phase (arrowhead).
(c) Although pb2A expresses two odorant receptors, both decay phases of the pb2A response to these stimuli arise from a single receptor (OR85e). When this receptor is mutated, only a small LFP response remains, and the subtracted trace shows both decay phases. (Blue trace: genotype is *Or46a-Gal4/UAS-DTl*. Magenta trace: genotype is *Or46a-Gal4/UAS-DTl; Or85e*$^{-/-}$. In both cases, DTl is used to kill the pb2B neuron.)
(d) Decay dynamics are receptor-specific, not neuron-specific. Here pb1A expresses both OR42a and OR47a. A stimulus that selectively activates OR42A (2-butanone 0.1×) produces overshoot, while a stimulus that selectively activates OR47A (pentyl acetate 0.02×) produces a second slow decay phase.

Based on these observations, we hypothesize that some odorant receptors couple to a secondary transduction pathway that is slower than the primary pathway. Overshoot after odor offset would be obscured in these neurons by a slow "shoulder" corresponding to this second pathway. The idea of a minor G-protein mediated transduction pathway has been suggested by several recent studies (Nakagawa et al. 2005 Science 307: 1638; Wicher et al. 2008 Nature 452:1007; Yao et al. 2010 J Neurosci 30:4562).

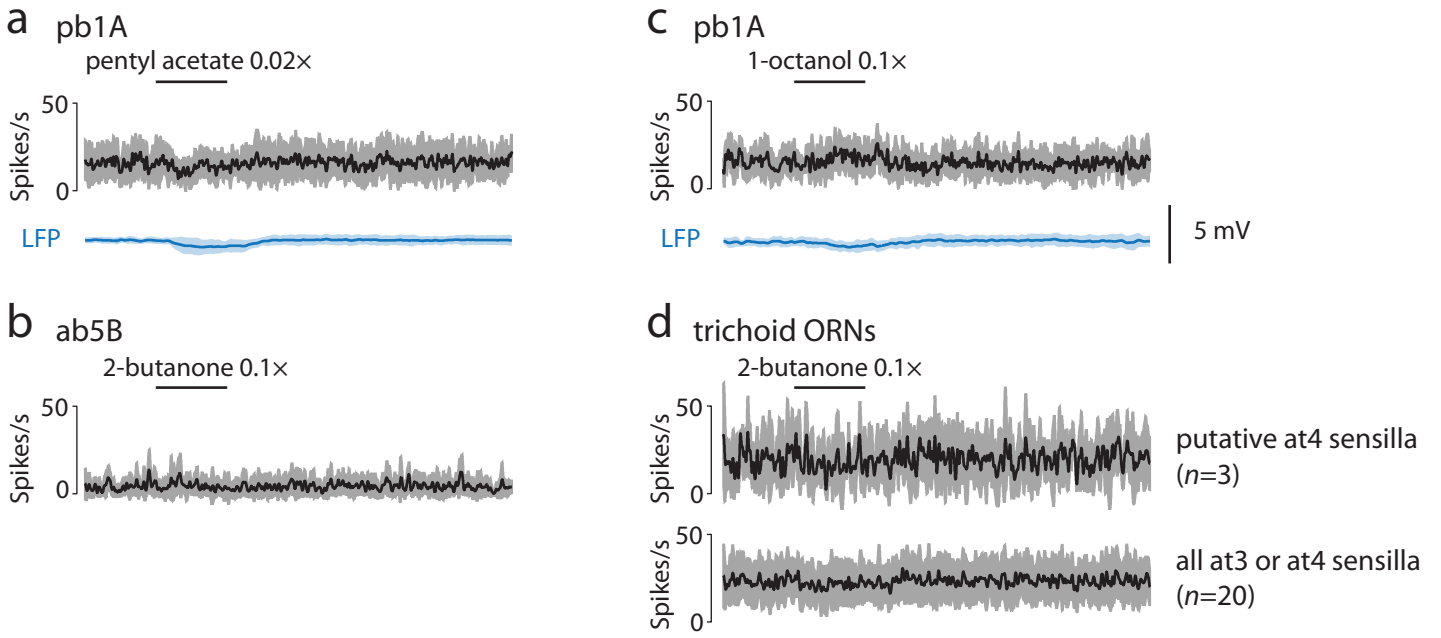

Supplementary Figure 5: Responses can be elicited independently through two odorant receptors co-expressed in the same ORN.

(a-b) In Figure 7a-b, we mis-expressed OR47a in the pb1A neuron, which natively expresses OR42a (Goldman et al., Neuron 45:661–666). We used selective odors to activate these two receptors independently in the same cell. The odors we used are 2-butanone (≤0.1×, selective for OR42a) and pentyl acetate (0.02×, selective for OR47a). Here we show that each of these odors is indeed selective for one of these two receptors.
(a) To test that pentyl acetate (0.02×) does not drive a response in OR42a, we recorded from control pb1A neurons that do not mis-express the second receptor. We saw no change in spike rate, and minimal change in the LFP in these recordings (n=7, mean ± s.d. across recordings). Genotype is *Or42a-Gal4/CyO*. This is one of the parental stocks used the generate the flies for Figure 7a-b.
(b) The neuron that natively expresses OR47a is the antennal ORN ab5B (Hallem et al. 2004 Cell 117:965–979). To test that 2-butanone (0.1×) does not drive a response in this receptor, we recorded from ab5B neurons. We saw no change in spike rate in these recordings (n=8). The LFP signal in this sensillum is not private to these ORNs, so it is not relevant to this control experiment. Genotype is *Or42a-Gal4/+;UAS-Or47a/+*. This is the same genotype used for Figure 7a-b.

(c-d) In Figure 7c-d, we mis-expressed a different receptor (OR47b) in the pb1A neuron. We used 1-octanol (0.1×) to inhibit OR47b, and we again used 2-butanone (0.1×) to activate OR42a. Here we show that each of these odors is indeed selective for one of these two receptors.
(c) To test that 1-octanol does not activate or inhibit OR42a, we again recorded from control pb1A neurons that do not mis-express a second receptor. We saw no change in spike rate and no LFP response in these recordings (n=7). (Genotype is again *Or42a-Gal4/CyO.)*
(d) The neuron that natively expresses OR47b is housed in the at4 sensillum, a trichoid sensillum on the antenna that contains three ORNs (Couto et al. 2005 Curr. Biol. 15:1535–1547). There are two trichoid sensillum types that contain three ORNs (at3 and at4), but they are not well-characterized. To test that 2-butanone (0.1×) does not drive a response in OR47b, we recorded randomly from many trichoids containing >2 waveforms, on the reasonable assumption that at4 sensilla comprise a significant fraction of all these sensilla. None of the trichoid sensilla we recorded from showed a significant change in spike rate in response to 2-butanone (≤0.1×). In 20 recordings, three sensilla showed clear inhibitory responses to 1-octanol (0.1×), suggesting that they were at4 sensilla. Firing rates in (d) represent unsorted multiunit activity. The LFP signal in these sensilla is not private to these ORNs, so it is not relevant to this experiment.

In sum, these experiments demonstrate that we can independently drive responses through two odorant receptors.

Nature Neuroscience: doi:10.1038/nn.2725

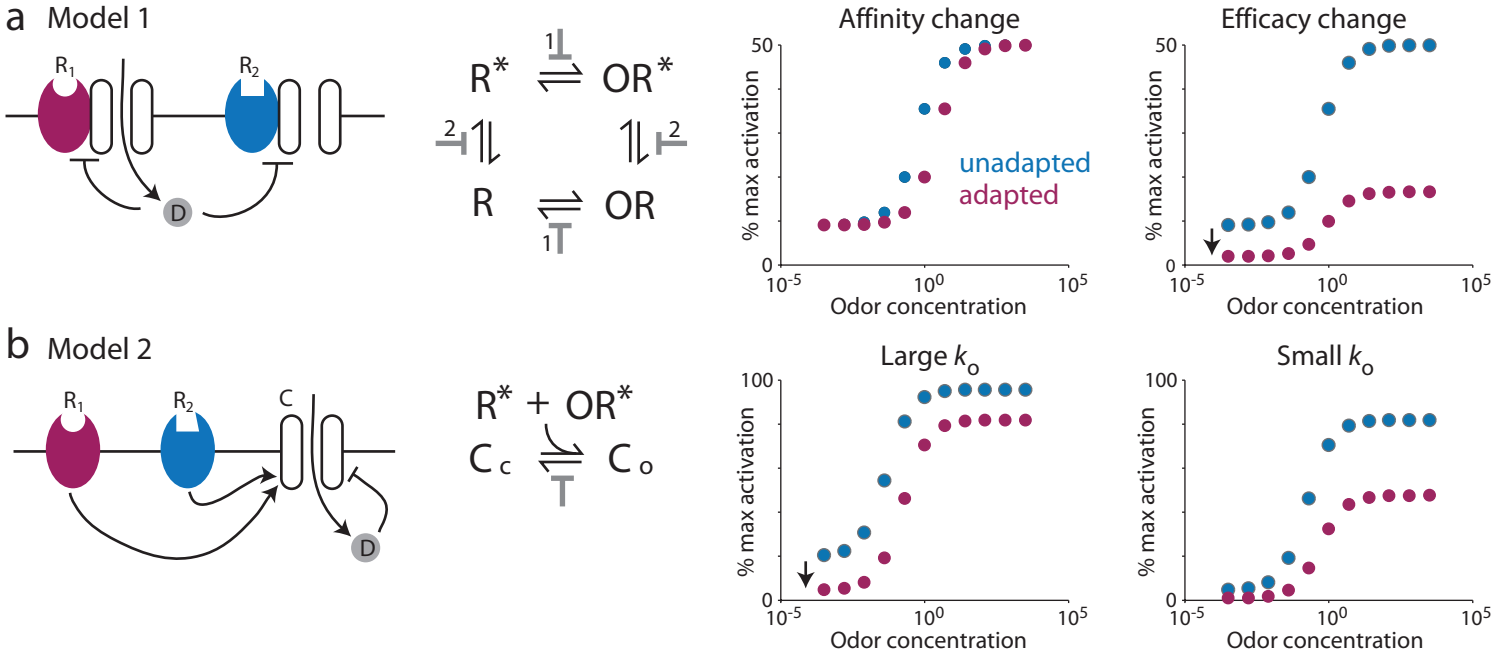

Supplementary Figure 6: Alternative models of transduction and adaptation.

(a) Model 1: The odorant receptor and OR83b form a ligand-gated channel. Transduction increases the concentration of a diffusible factor D, which decreases the affinity of the receptor for ligand (site 1 in the kinetic model) or the efficacy of receptor activation (site 2). Simulations (right) show the result of adaptation at these two sites on the concentration-response function. A decrease in affinity shifts the concentration-response function rightward, reminiscent of our result in Fig. 6e. However, a decrease in affinity cannot produce overshoot after odor offset. Conversely, a decrease in efficacy produces overshoot but not the rightward shift. Note the decrease in basal activity with adaptation in this simulation (arrow): this is the hallmark of overshoot.

(b) Model 2: Receptors associate dynamically with the transduction channel, and D decreases the ability of activated receptor to open the channel. This model predicts overshoot because adaptation decreases the ability of both OR* and R* to open the channel. Also, this model produces a rightward shift in the concentration-response function, provided that the rate constant for channel opening is large enough that the pool of activated receptors can fully activate most available channels at high odor concentrations.

Adaptation at any of the sites shown here for either model decreases transduction onset rate (not shown). Details of model implementation are described below.

Model 1: Here we assume receptor activation means channel opening. Rate constants are given by two parameters (k, s) where k specifies the odor-independent aspect of the equilibrium and s is a scaling factor that determines reaction speed. The activation rate constants for bound and unbound receptor (R and OR) differ by a constant (θ) which depends on odor and receptor. If $\theta>1$, the odor is excitatory because it stabilizes the active state (OR*). If $\theta<1$, the odor is inhibitory because it stabilizes the inactive state (OR). The binding rate constants for the active and inactive receptor (R* and R) differ by the same factor θ. Thus,

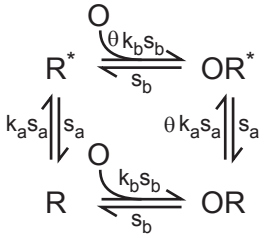

Note that this model assumes s_b is the same for active and inactive receptors and s_a is the same for bound and unbound receptors. This simplifies the implementation of the model, but the qualitative features of the model do not require these assumptions.

(continued on next page)

Supplementary Figure 6 (continued from previous page):

To simulate the effect of adaptation on binding affinity, we reduced the binding constant k_b by 5-fold, thereby shifting the equilibrium from bound toward unbound receptor, both for the active and inactive receptor states. To simulate the effect of adaptation on the efficacy of receptor activation, we reduced k_a by 5-fold, thereby shifting the equilibrium from active toward inactive receptor, both for the bound and unbound receptor states. Because it alters the equilibrium of unbound receptors, this type of adaptation decreases transduction even in the absence of odor. We set $k_a = 0.1$, $s_a = 10\ s^{-1}$, $k_b = 1\ M^{-1}$, $s_b = 100\ s^{-1}$, and $\theta = 10$. We chose k_a to produce a moderate level of spontaneous activity, and we chose a binding rate faster than the activation rate. Our qualitative results were not highly sensitive to these choices. All simulated odor pulses were 1-s step functions. The output of Model 1 was calculated using two matrices to describe dynamics in the presence and absence of odor:

$$\frac{d}{dt}\begin{bmatrix} R & R^* & OR & OR^* \end{bmatrix} = \begin{bmatrix} -(k_a s_a + [O]k_b s_b) & s_a & s_b & 0 \\ k_a s_a & -(s_a + [O]\theta k_b s_b) & 0 & s_b \\ [O]k_b s_b & 0 & -(s_b + \theta k_a s_a) & s_a \\ 0 & [O]\theta k_b s_b & \theta k_a s_a & -(s_a + s_b) \end{bmatrix} \begin{bmatrix} R \\ R^* \\ OR \\ OR^* \end{bmatrix}$$

where [O] is the concentration of odor in M. This was used as the dynamic input to Model 2.

Model 2: Here, the active receptor acts on the transduction channel to shift the equilibrium from closed channel (C_c) toward open channel (C_o):

$$C_c \underset{k_c}{\overset{[R^* + OR^*]\,k_o}{\rightleftharpoons}} C_o$$

We used Model 1 to specify receptor-ligand dynamics, and we modeled channel opening as a one-step process driven by active receptor (R*+OR*). To simulate the effect of adaptation on channel opening, we reduced k_o by a factor of 5. We explored two regimes for this model: a regime where virtually all channels are open at a saturating odor concentration (large initial k_o) and a regime where a substantial fraction of channels are closed at saturation (small initial k_o). For adaptation to produce a horizontal shift in the dose-response curve, two things must be true. First, the output of Model 1 must vary over a large dynamic range as the odor concentration is varied. To produce this larger range we set $k_a = 0.001$ and $\theta = 100$. Second, the equilibrium ratio k_o/k_c must be such that this range of (R*+OR*) drives channel opening over most of its dynamic range. In the first regime, $k_{o,\,initial} = 2500\ s^{-1}M^{-1}$ and $k_c = 10\ s^{-1}$, meaning almost all channels are open at saturating odor concentrations. In the second regime, $k_{o,\,initial} = 500\ s^{-1}M^{-1}$, meaning more channels are closed at saturation. Our qualitative results do not depend strongly on the other parameter choices. The output of Model 2 in response to the dynamic input provided by Model 1 is specified by an ordinary differential equation:

$$\frac{d}{dt}[C_o] = [R^* + OR^*]k_o[C_{total} - C_o] - k_c[C_o]$$

We approximated a solution to this equation using a fourth-order Runge-Kutta algorithm with a step size of 1 ms.

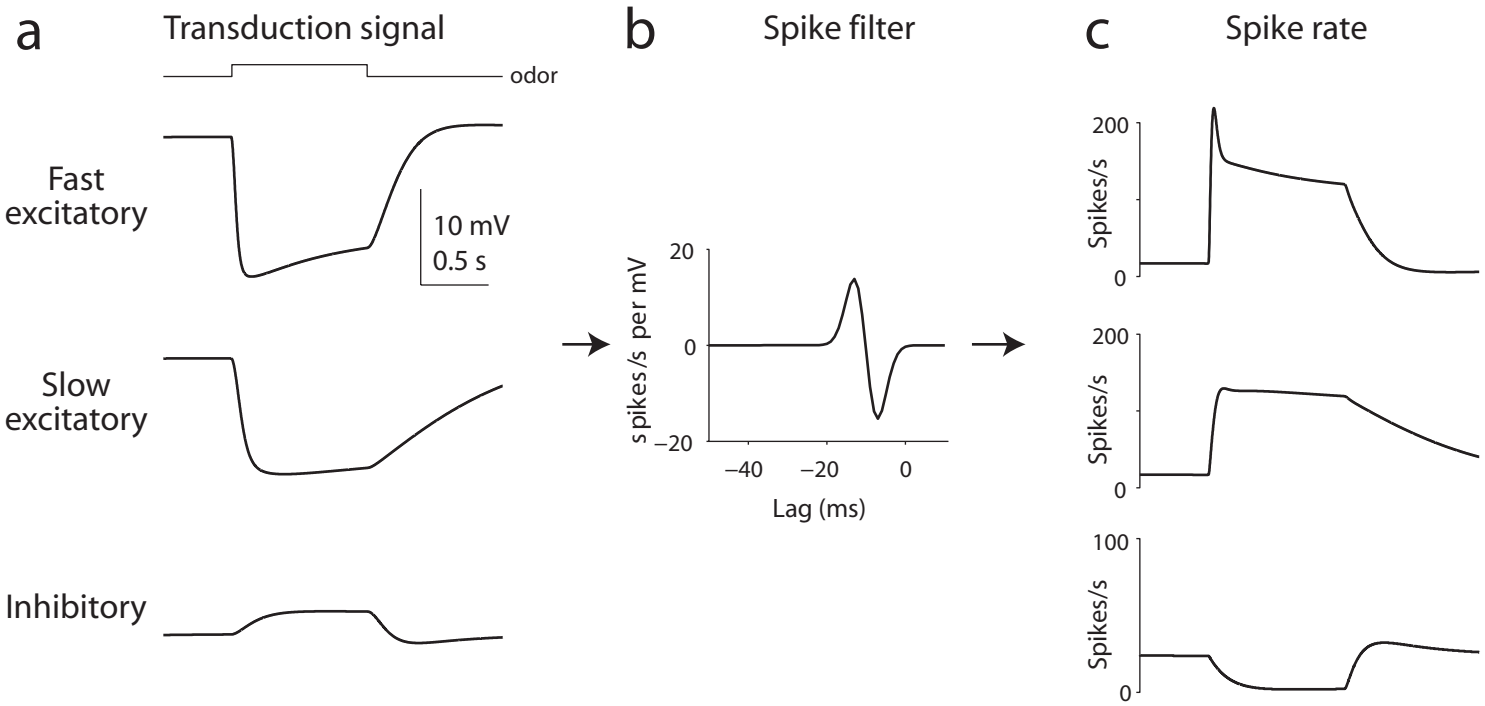

Supplementary Figure 7: Interaction of transduction and spiking.

A simple simulation illustrates how stepwise transformations through transduction and spiking can produce complex dynamics.
(a) The transduction signal is the output of Model 2 (from Supplementary Figure 6). Different odors were simulated by changing the rate constants in the model. Three combinations of rate constants are shown here.
(b) Transduction signals were convolved with an idealized biphasic spike filter (see Supplementary Figure 3a).
(c) The output of these two stepwise transformations recapitulates many of the qualitative observations shown in Figure 1.

Details of model implementation are described below.

Transduction: To generate the simulated transduction signals in (a) we first needed to model the time course of adaptation. We used Model 2 from Supplementary Figure 6 as the starting point for this. We assumed that adaptation is a negative feedback mechanism where a dynamic diffusible factor (D) grows slowly in proportion to the number of open transduction channels (C_O) at rate α, and is cleared in proportion to its own concentration at rate β:

$$\frac{d}{dt}[D] = \alpha[C_o] - \beta[D]$$

We set $\alpha = 0.8\ s^{-1}$ and $\beta = 0.6\ s^{-1}$. We chose these parameters because they produced results that qualitatively resembled the data. To simulate adaptation, the gating constant (k_o) was divided by [D]. To simulate a fast excitatory response, we used the parameters in Supplementary Figure 6 (Model 2, left graph). To simulate a slow excitatory response, we decreased s_a by 5-fold. To simulate an inhibitory odor, we used $\theta = 0.01$ (rather than 100) and we increased k_a from 0.001 to 0.002 in order to increase spontaneous activity and thereby increase the dynamic range for inhibition.

Spiking: The spike filter in (b) was created by multiplying a Gaussian function (mean -10 ms, standard deviation 3 ms) by a line with a slope of -8 and a y-intercept of 10.15 ms. This produces a differentiating filter with a slightly larger negative than positive lobe. The width of this filter was chosen to approximate that of the idealized filter in Supplementary Figure 3 (except that filter is sampled at 100 Hz, whereas this one is sampled at 1 kHz). The ratio of positive to negative lobe size was chosen to generate results that qualitatively resemble the data.

Nature Neuroscience: doi:10.1038/nn.2725